Dynamics of Brownian particles in three-dimensional ordered porous media subject to an oscillatory force

Shing Bor Chen*

Department of Chemical & Biomolecular Engineering, National University of Singapore, Singapore 117585

(Received 2 August 2015; revised manuscript received 9 October 2015; published 2 December 2015)

Brownian dynamics simulation has been employed to study the dynamic behavior of particles in three-dimensional ordered porous media subject to a sinusoidal force field. The media comprises interconnected spherical cavities arranged in a simple cubic lattice. The thermal noise assists the particles to undergo cavity hopping, leading to a displacement behavior analogous to stochastic resonance, when the imposed field is strong enough but not aligned with the aperture lines, and the oscillation frequency is not too high. The periodic mean trajectory depends on the strength, frequency, and orientation of the imposed field. At sufficiently large field strength, the periodic particle displacement can become nonsinusoidal due to the strong hindrance and pinning effect of the cavity wall.

DOI: 10.1103/PhysRevE.92.062105 PACS number(s): 05.40.Jc, 87.15.hg, 05.10.Gg

I. INTRODUCTION

Stochastic resonance (SR), a phenomenon where an input signal is amplified due to thermal noise in the system, has been observed in different disciplines, and found applications in optical, electronic, magnetic, and neuronal systems [1]. It arises from synchronization between noise-induced hopping and an external periodic driving force, allowing the system to circumvent a barrier that can be either energetic, entropic, or purely geometric. The entropic or geometric barrier is often encountered in soft matter and biological systems, where particles migrate in a constrained environment such as porous media, gels, ion channels, etc. [2–6]. In this paper, we investigate the dynamic behavior of Brownian particles in three-dimensional (3D) ordered porous media subject to an imposed sinusoidal force field.

Transport of particles or molecules in porous media is involved in many applications, such as chromatography, catalysis, gel electrophoresis, etc. Their behavior depends largely on the media porosity and microstructure and their nonbonded interaction with the media. As such, particles, when made fluorescent for example, can serve as tracers to explore and measure the properties of porous media. To understand the relation between particle transport and dynamics and porous media structure, it is preferable to use ordered porous media because of a well-defined pore shape and arrangement periodicity. Such media have been realized via bottom-up self-assembly and microfluidic techniques to fabricate colloidal crystals or their inverted counterparts [7–9]. For orderly connected cavities, particle diffusion [10–13] and migration under a constant external field [14–19] have been investigated. These media are regarded as open systems because of the structural periodicity.

For oscillatory external fields, closed cavity systems are often considered in most of the studies focusing on SR. Burada *et al.* [4] investigated entropic SR using the dynamics of a Brownian particle confined in a closed 2D structure (two connected cavities) subjected to a sinusoidal force along the structure axis and a constant force in the transversal direction, which can break symmetry to push the particle to one side of the cavities. The structure, which is defined by a quartic double-well function, has a smoothly varying width and is symmetric about the central narrow neck with a finite length. The dynamics is governed by the overdamped Langevin equation and the reflecting boundary condition at the structure wall. They found that the entropic effect originating from the confinement and the boundary irregularity leads to an effective bistable potential and hence the entropic SR, showing an optimal noise level for arrival at the greatest spectral amplification at a given frequency. The effective bistable potential, however, is not found in the case of sharp confining geometries [5], for example, compartments or cavities in septate channels separated by zero-thickness partition walls, where holes are pierced at the center. Ghosh *et al.* [5] studied such cases by examining the dynamics of Brownian particles in a 2D rectangular box divided by a zero-thickness partition wall with a small central hole. The sinusoidal external force is applied in the direction parallel to the main channel axis. They called the attained amplification geometric SR, which is distinct from the entropic SR and can occur at low enough frequency and large enough field strength. The investigation was later extended to cases with other directions of the imposed field [6]. In all these studies, particles are confined in 2D closed cavity systems.

In view of the practicality of 3D continuous ordered porous media (open systems), we are motivated to investigate the dynamics of Brownian particles in such media subject to an oscillatory external field (e.g., an electric field) and explore the possibility of observing an analogy of SR. In the present work, Brownian dynamics (BD) simulation will be conducted to calculate the mean particle trajectory at varied field strength, orientation, and frequency.

II. METHOD

We consider 3D ordered porous media constructed by interconnected spherical cavities arranged in a simple cubic (sc) lattice as shown in Fig. 1. The radius of each cavity is a, and the diameter of aperture between two adjacent cavities is $2b$. Due to the periodicity of the ordered structure, only one cavity

*checsb@nus.edu.sg

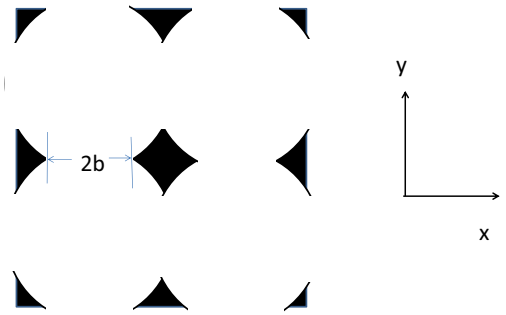

FIG. 1. (Color online) Schematic of connected spherical cavities with radius a arranged in SC lattice.

needs to be placed in a cubic simulation box with side length equal to L. Periodic boundary conditions are implemented in the simulation as usual. In this study, we consider cases with $b \ll a$, so L is nearly equal to the cavity diameter $2a$.

In the present study, the particle is assumed to be much smaller in size than the aperture and can hence be approximated as a point. The dynamics of the particle is described by the overdamped Langevin equation [20]:

$$\zeta \frac{d\mathbf{r}}{dt} = \mathbf{F} + \mathbf{R} \tag{1}$$

where ζ is the friction coefficient, $\mathbf{r}$ is the particle position vector, $\mathbf{F} = \mathbf{F_0}\cos(2\pi\omega t)$ is the imposed oscillatory force with ω being the frequency, and $\mathbf{R}$ is the random force due to the incessant collision of the solvent molecules with the particle. We apply Euler's method to numerically integrate Eq. (1) to arrive at the location change [13,18–20]

$$\Delta\mathbf{r} = \frac{\mathbf{F}}{\zeta}\Delta t + \left(\frac{2k_BT}{\zeta}\right)^{1/2}\Delta\mathbf{W}, \tag{2}$$

where Δt is the time step, and $\mathbf{W}$ is a Wiener process with the increment being

$$\Delta W_i = (12\Delta t)^{1/2}\left(\xi_i - \frac{1}{2}\right) \tag{3}$$

The distribution of the random number ξ_i is uniform in [0,1] with $i = x$, y, or z. We handle the impermeability of the solid mass by implementing the reflecting boundary condition [13,18,19].

Hereafter, we normalize all lengths by L and time by L^2/D_0, where $D_0 = k_BT/\zeta$ is the self-diffusion coefficient of the particle in pure solvent. As such, Eq. (2) becomes dimensionless as

$$\Delta\mathbf{r} = \frac{LF_0}{k_BT}\cos(2\pi\omega t)\Delta t\mathbf{e} + (24\Delta t)^{1/2}\mathbf{s}, \tag{4}$$

where $\mathbf{e}$ is the unit vector describing the direction of the external force, and the vector $\mathbf{s}$ has components given by

$$s_i = \left(\xi_i - \frac{1}{2}\right).$$

In this study, we consider the imposed field to be parallel to the xy plane and form an angle θ from the x direction, i.e., $\mathbf{e}\cdot\mathbf{e}_x = \cos\theta$ and $\mathbf{e}\cdot\mathbf{e}_z = 0$. New coordinates x' and y' are defined via rotating the x and y axes by the angle θ in the counterclockwise direction such that $\mathbf{e}$ is in the x' direction. The dimensionless parameter LF_0/k_BT is designated as Pe′, which measures the relative importance of the external field to thermal noise. The time step $\Delta t = 10^{-6}$ is used to compute the particle trajectory. For each run, we placed 50000 noninterfering particles in order to take the ensemble average for a better accuracy. Their initial locations are fixed at the cavity center. The mean displacement along the direction of $\mathbf{F_0}$ can be calculated as a function of time by

$$C = \langle[\mathbf{r}(t) - \mathbf{r}(0)]\cdot\mathbf{e}\rangle, \tag{5}$$

where $\langle\cdot\rangle$ denotes an ensemble average over the 50000 particles. Larger numbers of particles, such as 100000 and 200000, have also been tried, and we observe only negligible change in results (see the Appendix). For non-Brownian particles, we set the second term on the right side of Eq. (4) to zero, and treat Pe′ as a nominal parameter representing the field strength. To map to a realistic aqueous system, we consider particles with radius of 10 nm in cavities with diameter of 1 μm under an electric field $F_0 = 10\,\mathrm{V/cm}$ at 10 Hz. Using the typical surface charge density 15 $\mu\mathrm{C/cm}^2$, we find $\mathrm{Pe}' = 45.8$ and $\omega = 0.46$ at room temperature.

III. RESULTS AND DISCUSSION

The arrangement of cavities in sc lattices as shown in Fig. 1 features three principal directions x, y, and z as regards the nearest neighbor. These are also the directions for the so-called aperture lines designated in this study. The length ratio $S = b/a$ is fixed at 0.1, for which $a = 0.502$. For all cases investigated in the present study, the average particle trajectories are observed to be always periodic, although the baseline may slightly deviate from zero. The periodicity has been checked and confirmed for $t \geqslant \omega^{-1}$ by simulations up to 100 periods for $\omega = 10$. As such, we will present each average trajectory only in the second and third periods for illustration. Error analysis of the amplitude data obtained is presented in the Appendix.

A. External field parallel to aperture lines

We first consider the case with $\theta = 0$, where the imposed field is parallel to a group of aperture lines. For a non-Brownian particle in pure solvent under the same oscillatory field, the displacement can be determined analytically by integrating Eq. (1) without the second term on the right side, to yield $C = (\mathrm{Pe}'/2\pi\omega)\sin(2\pi\omega t)$. Note that this analytic expression is also the mean trajectory of Brownian particles in pure solvent without any constrictions. In the porous media, our simulation results find that the mean displacement C always shows sinusoidal time dependence, although the baseline, which is found to be independent of time, may shift very slightly away from zero. As such, the amplitude is determined by $A = (C_{\max} - C_{\min})/2$. Figure 2(a) presents the variation of the normalized amplitude A/A_0 with Pe′ for $\omega = 0.1$, 1, and 10, where $A_0 = \mathrm{Pe}'/2\pi\omega$ is the amplitude for the corresponding non-Brownian particles, which move along the aperture lines and will never hit the wall in this case. Brownian particles, to the contrary, may diffuse away from the aperture line and possibly encounter the cavity wall. The

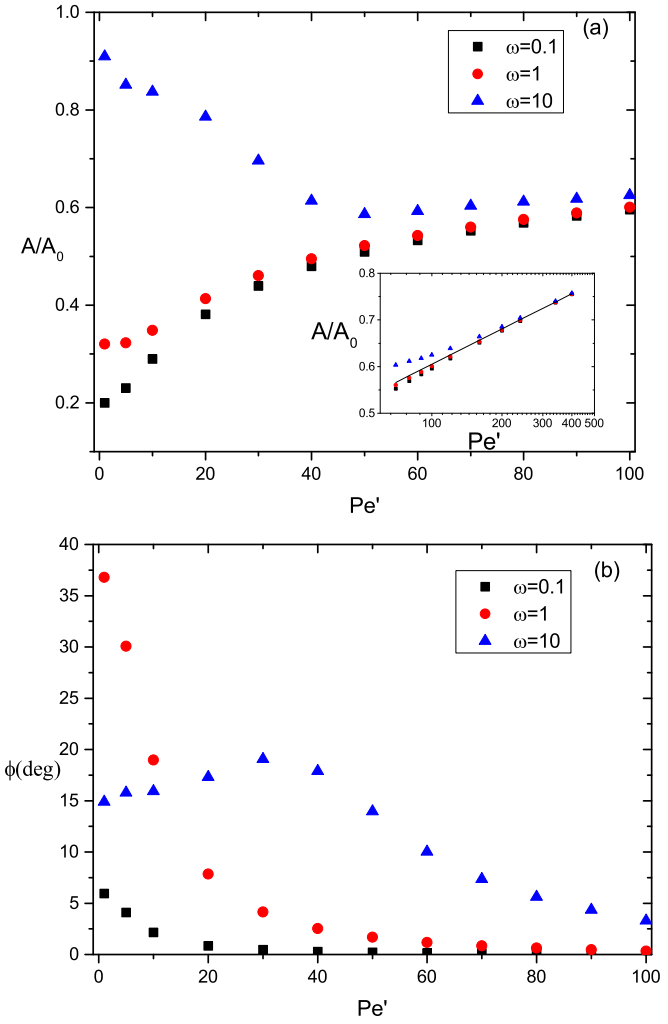

FIG. 2. (Color online) (a) Normalized amplitude and (b) phase shift as a function of Pe′ for $\theta = 0$.

hindrance effect of solid mass renders A always smaller than A_0 as clearly seen in the figure, and is expected to approach A_0 as $\mathrm{Pe}' \to \infty$. As mentioned earlier, SR features signal amplification as compared to the counterpart system in the absence of any thermal motion whatsoever (non-Brownian particles). Therefore we conclude that nothing similar to SR occurs when the imposed field is in any of the three principal directions. We have also examined the corresponding cases where the particles initially are randomly located in the cavity, and found that the results hardly change.

At $\omega = 0.1$ and 1, A/A_0 is found to increase with Pe′. At $\omega = 10$, however, A/A_0 first decreases, reaches a very weak minimum, and then increases. It should be noted that, unlike A/A_0, A always increases with Pe′. The interesting difference in the behavior of A/A_0 for small enough Pe′ at $\omega = 10$ can be explained by the fast field oscillation with time scale $\omega^{-1} \ll \mathrm{Pe}'^{-1}$, where each reversal of field direction takes place before significant wall-reflecting effect can result. For large Pe′ ($\gg\omega$), the particles can go through the hit-rebound-escape process several times prior to each field reversal. The movement behavior is hence similar to that subject to an external field with constant strength and direction, which was investigated in our prior study [18] via computation of effective velocity and mean first-passage time. That study showed that for large Pe′ V/V_0 depends on Pe′ logarithmically, where V is the average velocity and V_0 is the corresponding velocity in pure solvent. One can see a similar behavior for A/A_0 from the inset of Fig. 2(a), where the fitting line is $A/A_0 = 0.103 + 0.251 \log_{10} \mathrm{Pe}'$.

In addition to the result $A/A_0 < 1$, there could be a phase shift ϕ for the periodic displacement displaying the time dependence in terms of $\sin(2\pi\omega t + \varphi)$, and the ϕ result is shown in Fig. 2(b). At large Pe′, most of the particles are driven into and then moving along an obstacle-free cylindrical zone with radius $\sim b$ along the aperture line [18,19] because they can hardly drift away via the very weak random motion. The situation is somewhat analogous to the case in pure solvent, and therefore the phase shift becomes very small towards zero. At small Pe′, however, the phase shift could be significant, e.g., $\sim 37^\circ$ at $\mathrm{Pe}' = 1$ and $\omega = 1$. For $\omega = 0.1$ and 10, the phase shift reduces to $\sim 6^\circ$ and $\sim 15^\circ$, respectively, at this Pe′.

To check whether the phase shift arises from the reflecting boundary condition adopted, we also try the other commonly used boundary condition—the rejection condition whereby a move leading to particle penetration into the solid mass is unacceptable, and the preceding position is retained. Quantitatively similar results are obtained. To understand this interesting phase shift phenomenon, we examine two related cases: (1) the mean trajectory of Brownian particles at the same Pe′ in pure solvent, and (2) the mean trajectory of non-Brownian particles with random initial positions in porous media. No phase shift is observed for either case, indicating the necessity of both random force and cavity surface for the occurrence of this phenomenon.

We propose the following explanation for the observed phase shift. For O(1) Pe′, the migration and diffusion rates are comparable in principle. However, due to the sinusoidal nature of the imposed field, there exist short time intervals around $t = (2n + 1)/4\omega$, with n an integer, during which the imposed field is vanishing and becomes weaker than the random force. As such, the obstruction effect of the cavity wall along with the dominating Brownian motion can facilitate the reverse movement of the particles and hence a biased distribution before the imposed field changes its direction, thereby leading to the positive phase shift.

B. External field not along aperture lines

Now we consider cases with $\sin^{-1} S < \theta \leqslant 45^\circ$, where the imposed field does not align with any aperture lines, and hence the obstruction effect of the cavity wall is expected to be significant. In fact, the no-penetration condition at the cavity surface will cause non-Brownian particles to eventually oscillate along the diameter path parallel to $\mathbf{F}_0$, thereby leading to permanent particle entrapment inside the cavity. This is illustrated in Fig. 3 which plots the mean trajectories for $\omega = 1$ and nominal $\mathrm{Pe}' = 10$, 30, and 80. One can see that with increasing Pe′, the time spans during which the particles are pinned to the wall (i.e., $C = \pm 0.502$) are longer. The trajectory indeed will approach a square wave as $\mathrm{Pe}' \to \infty$.

For Brownian particles, random motion is the mechanism allowing them to deviate from this trapping trajectory and

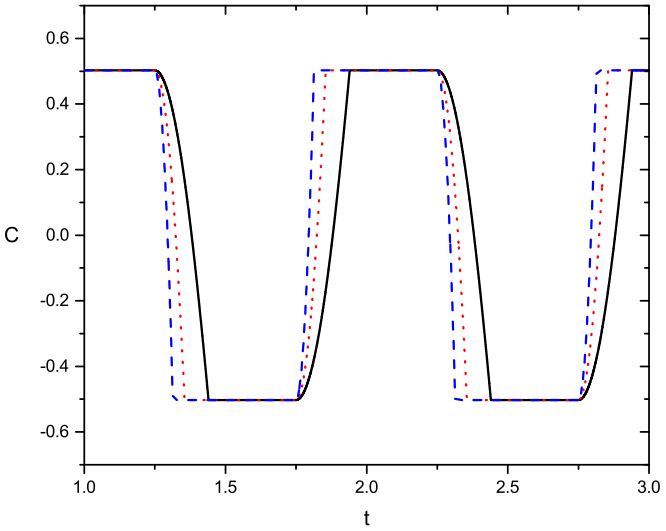

FIG. 3. (Color online) Trajectory of non-Brownian particles for $\mathrm{Pe}' = 10$ (solid line), 30 (dotted line), and 80 (dashed line) at $\omega = 1$ and $\sin^{-1} S < \theta \leqslant 45^\circ$.

escape from one cavity to another. Figures 4(a)–4(c) plot C for $\theta = 45^\circ$, $\omega = 0.1$, 1 and 10, respectively. One can see that at $Pe' = 10$, the mean displacement is sinusoidal. In contrast, when the imposed field becomes strong enough, the mean displacement, despite remaining periodic, is no longer sinusoidal. For $\theta = 20^\circ$ and 30°; representative results are shown in Fig. 8 (in the Appendix) for comparison. The deviation can become substantial at large Pe'. In view of the different, large deviations for various cases, we chose to present A/A_0 with $A = (C_{\max} - C_{\min})/2$ and $A_0 = \min(\mathrm{Pe}'/2\pi\omega, a)$, instead of examining the amplitude of the first harmonic of the Fourier expansion of the trajectory in a spectral signal analysis [4–6]. A brief discussion on this matter is given in the Appendix. Figures 5(a)–5(c) show the variation of A/A_0 with Pe' for different θ at $\omega = 0.1$, 1, and 10, respectively. One can see that stochastic resonance ($A/A_0 > 1$) can take place for low enough frequency and high enough field strength, similarly to the finding for geometric SR [5,6]. The prominence of these phenomena both decrease with increasing ω and θ. Since $A/A_0 \to 1$ as $\mathrm{Pe}' \to \infty$ (no thermal noise), there should exist a local maximum of A/A_0 at large enough Pe' for those cases where such an expected behavior is not yet seen in Fig. 5. However, further increase in Pe' would require the use of smaller Δt and hence render the simulation more time consuming.

A subtle issue arises for $\theta \neq 0^\circ$ or 45°. Our prior study [18] on the force-driven migration of Brownian particles subject to a steady external field found that the mean trajectory does not necessarily align with the imposed field. The mean trajectory orientation θ_V can be written as $\theta_V = \theta + \Delta\theta$, where $\Delta\theta$ is found to be negative, and $|\Delta\theta|$ increases with Pe' (see Fig. 5 of Ref. [18]). For the oscillatory field in the present work, the orientation behavior is expected to become more complicated. We calculate $\Delta\theta = \tan^{-1}(\langle y' \rangle / \langle x' \rangle)$ at each time point and plot the case of $\mathrm{Pe}' = 80$ in Figs. 6(a) and 6(b) for $\omega = 0.1$ and 1, respectively. The sharp peaks and valleys are due to vanishing $\langle x' \rangle$ (i.e., $C \approx 0$) in the periodic trajectory [cf. Figs. 4(a) and 4(b) for $\theta = 45^\circ$], and thus do not deserve special attention. For $\theta = 20^\circ$ and 30°, negative $\Delta\theta$ is shown by the part showing more gradual variation, whereas $\Delta\theta$ vanishes for $\theta = 45^\circ$. To make comparison, we also performed the simulation for the case of a steady imposed field at $\mathrm{Pe}' = 80$ and found that $\Delta\theta$ is a constant equal to -19.4°, -26°, and nearly zero for $\theta = 20^\circ$, 30°, and 45°, respectively. In view

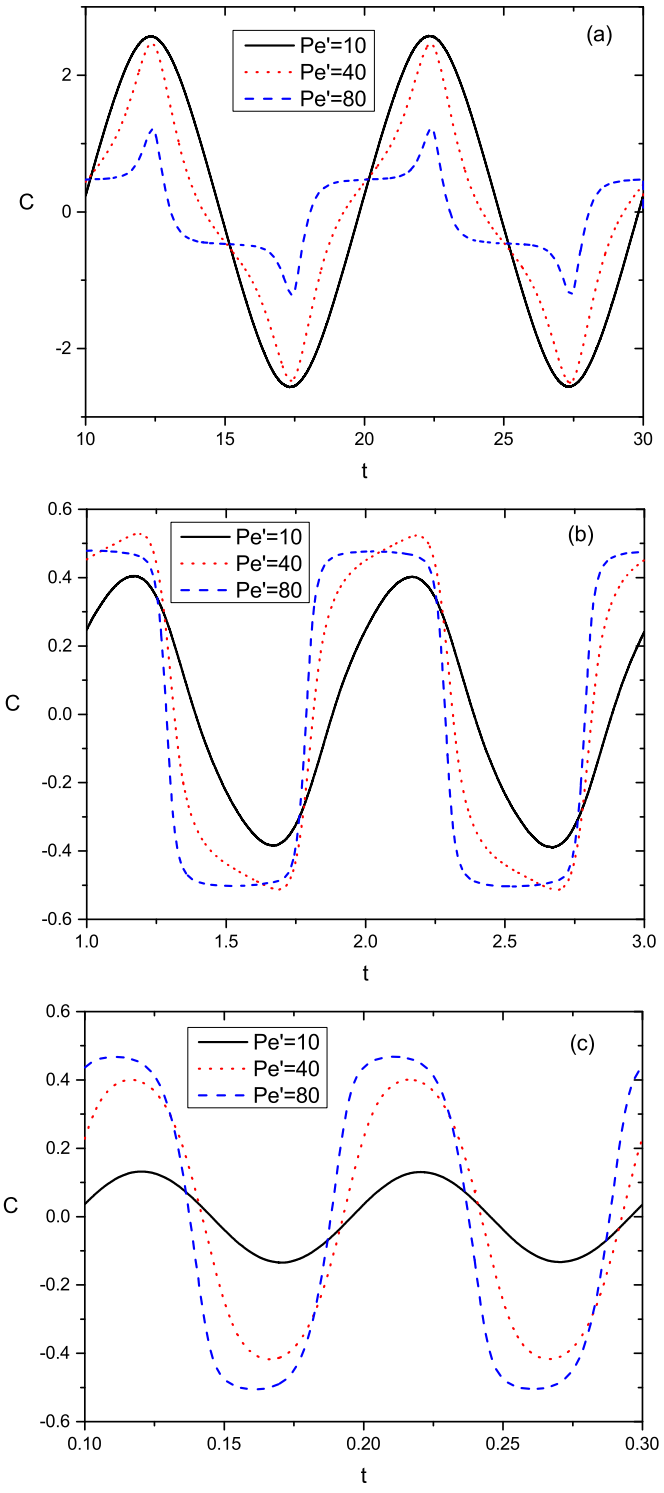

FIG. 4. (Color online) Mean trajectory of Brownian particles for $\theta = 45^\circ$ and $\omega =$ (a) 0.1, (b) 1, and (c) 10.

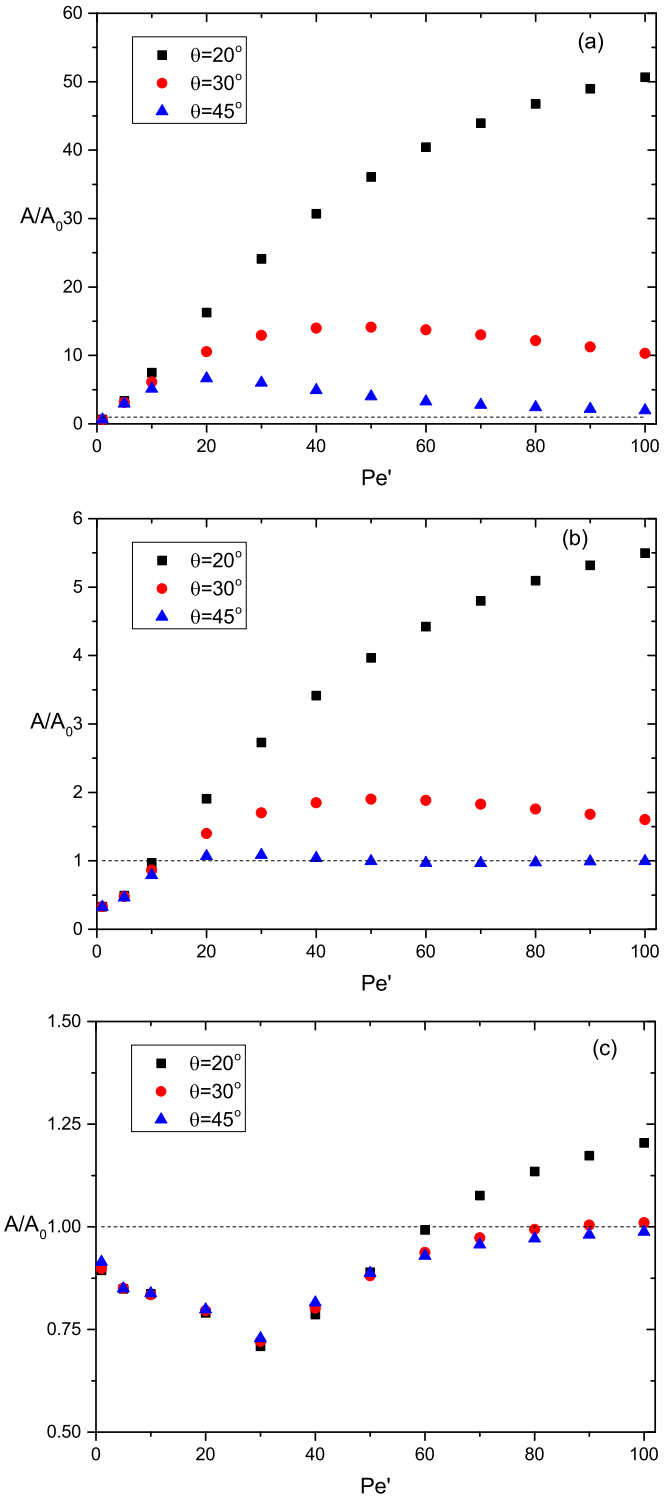

FIG. 5. (Color online) Normalized amplitude as a function of Pe′ for $\omega =$ (a) 0.1, (b) 1, and (c) 10.

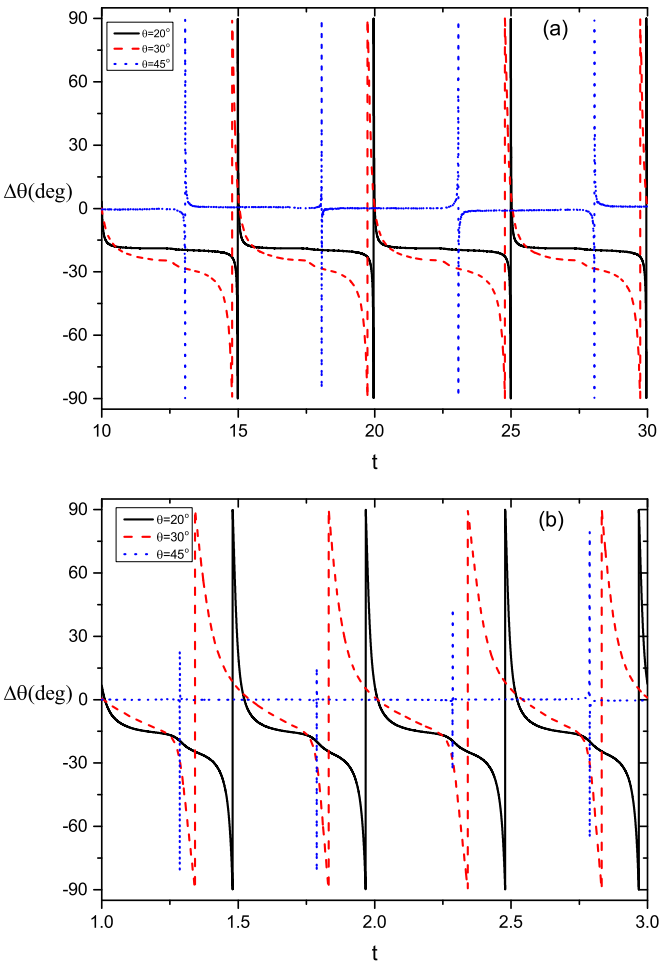

FIG. 6. (Color online) Angle deviation as a function of time for Pe′ = 80 and $\omega =$ (a) 0.1 and (b) 1.

of the complex $\Delta\theta$ in the oscillatory field, we have chosen to examine A/A_0 based on the displacement projection on **e**, i.e., Eq. (5) for simplicity.

When $\omega >$ Pe′$/2\pi a$, the imposed field oscillates too rapidly to drive the particles to impact the wall and experience its effect for a sufficient time before each direction reversal of the imposed field. As seen in Fig. 5(c), the decreasing trend of A/A_0 with Pe′ for Pe′ < 30 at $\omega = 10$ somewhat resembles that for $\theta = 0°$ at the same frequency shown in Fig. 2(a). Moreover, the trajectory remains sinusoidal for Pe′ $= 10$ and nearly sinusoidal for Pe′ $= 40$ or even 80 when $\theta = 45°$ [see Fig. 4(c)]. From these findings and comparison, we conclude that under a fast oscillatory field, the solid mass merely causes hindrance and perturbation to the particle movement as compared with the case in pure solvent, and hence $A < A_0$ can be accounted for.

For $\omega \ll$ Pe′$/2\pi a$, on the other hand, slow oscillation allows the particles a sufficient time to impinge on the wall and undergo the hit-rebound process a number of times. Therefore they may have a chance to escape the cavity via the aperture. This wall effect is most pronounced for $\theta = 45°$ because particles have to travel a longer distance to reach the aperture than for other values of θ. Figure 4(a) has clearly revealed the aforementioned process, in particular for the case of Pe′ $= 80$ and $\omega = 0.1$: particles are pinned to the cavity wall for considerable time spans ($C = \pm 0.502$), and each peak and valley in between indicates escape and the following movement reversal. When ω is increased to 1, the likelihood of escape is lessened due to the reduction in time allowed for this process, and hence $|C|$ can exceed 0.502 only slightly.

Stochastic resonance cannot even occur for lower Pe′ or greater ω as shown in Figs. 4(b) and 4(c).

For smaller θ, the required travel distance to the nearest aperture for escape becomes shorter, thereby increasing the fleeing ease and possibility. A/A_0 can get as large as 50 for $\theta = 20^\circ$, Pe′ $= 100$, and $\omega = 0.1$. In our prior study [18], the mean passage time of particles which are randomly located initially in a spherical cavity with one single aperture subject to a constant imposed field was computed from BD simulation to investigate the time required for escape. One can see from Fig. 8 of Ref. [18] that, for $S = 0.3$, the mean first-passage time decreases and then increases with Pe′ when $\theta \geqslant 30^\circ$, and this behavior is more pronounced for larger θ. The time ratio of $\theta = 45^\circ$ to $\theta = 30^\circ$ was found to increase with Pe′ and reach about 150 already at Pe′ $= 60$. The strong θ dependence of the escape time can explain why the stochastic resonance is considerably stronger for $\theta = 20^\circ$ than for $\theta = 30^\circ$ and 45° as shown in Fig. 5. The prolonged stay of particles in the cavity is associated with the wall-pinning effect. When the particles are pushed to the cavity wall by a strong field, they rebound in such a way as to migrate towards the location to which the field points from the cavity center [18,19]. The imposed field hence restrains the effective lateral Brownian motion, which is required for the particle escape as mentioned earlier.

To verify this thought, we calculate two components of the mean square displacement (relative to the migration) perpendicular to the imposed field:

$$d_1 = \langle y'^2(t)\rangle - \langle y'(t)\rangle^2,$$
$$d_2 = \langle z^2(t)\rangle - \langle z(t)\rangle^2.$$

The results for $\omega = 0.1$ and Pe′ $= 80$ are presented in Fig. 7(a). It can be seen that d_1 is much greater than d_2 (inset) in these cases, indicating that the particle escape is primarily via the random motion in the y' direction. For each curve, the local slope can be viewed as the effective diffusivity at the corresponding time point. For d_2, there exist time spans in which the slope is nearly zero, indicative of very weak diffusion. In between, a more pronounced change in d_2 is observed. This behavior is also found for d_1 when $\theta = 45^\circ$. The sharper increase takes place around the time points of field reversal [$t = (2n+1)/4\omega$], where the random motion becomes stronger than the migration driven by the diminishing field, and thus the wall-pinning effect is weakened considerably. This phenomenon, however, does not to happen to d_1 for $\theta = 20^\circ$ and 30°, where the slope variation appears rather smooth in contrast.

To gain a better understanding, we calculate d_1 and d_2 for the corresponding cases with a steady imposed field (Pe′ $= 80$), and the results are shown in Fig. 10 (in the Appendix). We find that although d_1 continues to dominate over d_2, both are linear functions of time, as opposed to the behavior in the oscillatory field. The slope of d_1 is found to be very small ($\sim$0.0074) for $\theta = 45^\circ$, which is comparable to 0.012 for the nearly horizontal parts in Fig. 7(a). For the steady field with $\theta = 20^\circ$ and 30°, the slope increases substantially to 0.88 and 0.41, respectively. Moreover, one can see from Fig. 5(a) that, while $A/A_0 = 2.4$ for $\theta = 45^\circ$ (Pe′ $= 80$), it increases to about 12 and 47 for $\theta = 30^\circ$ and $\theta = 20^\circ$. This stark difference is also evident from the trajectory plots for Pe′ $= 80$ in Figs. 4(a) and 8. It means that

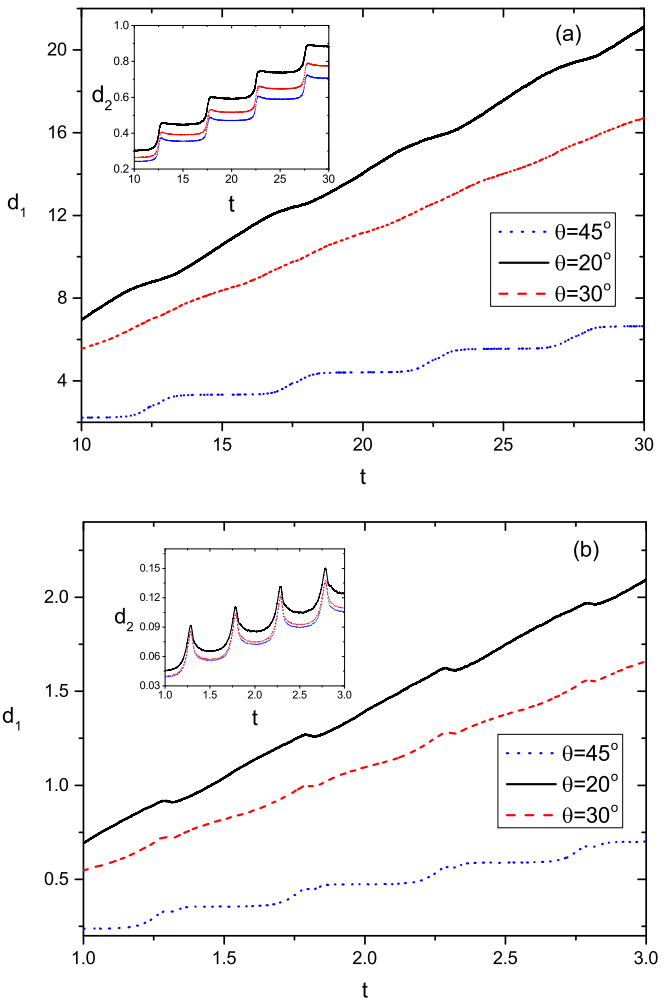

FIG. 7. (Color online) Components of mean square displacement of Brownian particles for Pe′ $= 80$ and $\omega =$ (a) 0.1 and (b) 1. Curves from top to bottom are for $\theta = 20^\circ$, 30°, and 45°.

for $\theta = 45^\circ$, the particles on average move merely from one cavity to the other shortly prior to each field reversal, whereas they can travel through many cavities in contrast for $\theta = 30^\circ$ and $\theta = 20^\circ$. For these two angle values, the escape time becomes too short to manifest itself in Figs. 7(a) and 8. To assess the hindrance in diffusion, we calculate $\Delta d_1/\Delta t$ and $\Delta d_2/\Delta t$ over the two periods to find the values 0.708 and 0.0289 for $\theta = 20^\circ$; 0.557 and 0.0255 for $\theta = 30^\circ$; 0.221 and 0.0231 for $\theta = 45^\circ$. These values are all smaller than 2, which is the slope of the straight line for corresponding diffusion in pure solvent.

Figure 7(b) plots d_1 and d_2 against time at $\omega = 1$ and Pe′ $= 80$ to show the difference in behavior at higher frequency. Interesting complications arising from the faster field oscillation can be observed. Despite remaining small, d_2 shows a stronger wavy characteristic. For d_1, there are kinks in each curve shortly behind the time points of field reversal. The values of $\Delta d_1/\Delta t$ and $\Delta d_2/\Delta t$ are 0.7 and 0.0395 for $\theta = 20^\circ$; 0.557 and 0.0347 for $\theta = 30^\circ$; 0.231 and 0.0333 for $\theta = 45^\circ$. In comparison with those for $\omega = 0.1$, $\Delta d_2/\Delta t$ is found to become larger, while $\Delta d_1/\Delta t$ remains nearly unchanged.

TABLE I. Normalized amplitude for $\theta = 20^\circ$ and $\omega = 10$.

Pe′	A/A_0
1	0.872 ± 0.032
10	0.831 ± 0.005
50	0.890 ± 0.002
100	1.207 ± 0.002

IV. CONCLUSION

BD simulation has been employed to investigate the dynamic behavior of Brownian particles in 3D ordered porous media (open system) subject to a sinusoidal external force. The amplitude of mean displacement can be enhanced and attain a maximum when the imposed field does not align with any aperture lines, as well as at sufficiently low frequency and large enough field strength. This phenomenon arises from the thermal noise that assists the particles to hop from one cavity to another through an aperture, leading to an increased displacement as compared to the entrapment of the non-Brownian counterparts in one cavity. Such enhancement resembles SR in closed system. The prominence of this behavior depends on the frequency, field strength, and field orientation relative to the aperture lines.

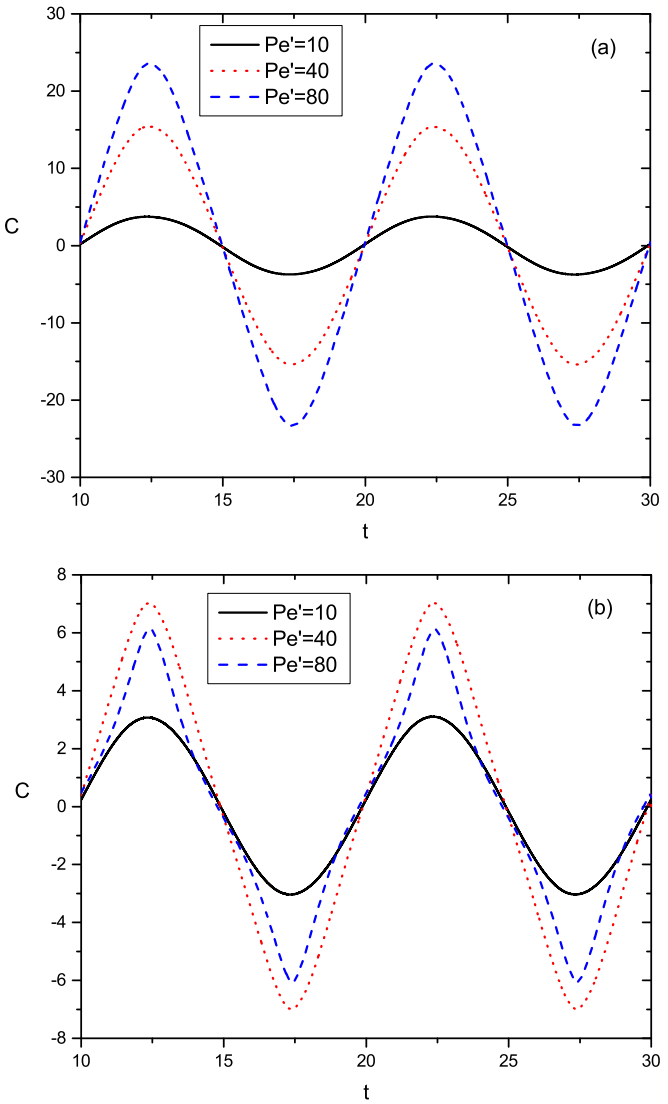

FIG. 8. (Color online) Mean trajectory at $\omega = 0.1$ for (a) $\theta = 20^\circ$ and (b) $\theta = 30^\circ$.

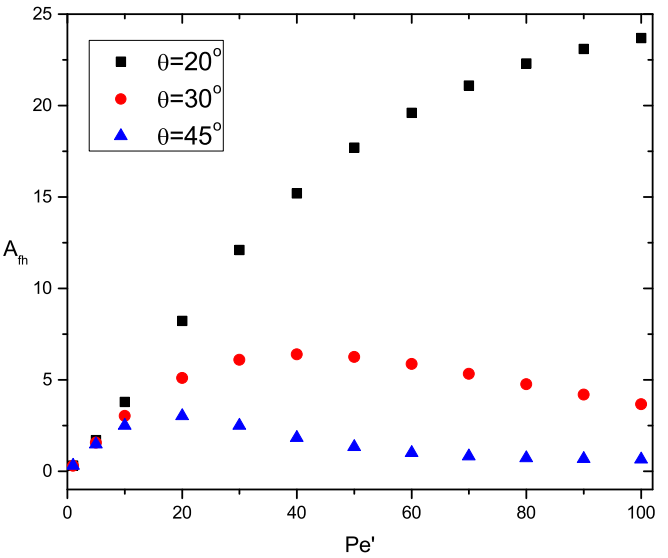

FIG. 9. (Color online) Amplitude of first harmonic of Fourier expansion of trajectory for $\omega = 0.1$.

ACKNOWLEDGMENT

This work was financially supported by National University of Singapore through Grant No. R-279-000-352-112.

APPENDIX: DATA ERROR ANALYSIS AND SUPPLEMENTARY RESULTS

Error analysis of the simulation data is demonstrated for the case of $\theta = 20^\circ$ and $\omega = 10$. We carry out five independent runs to determine the mean normalized amplitude and the

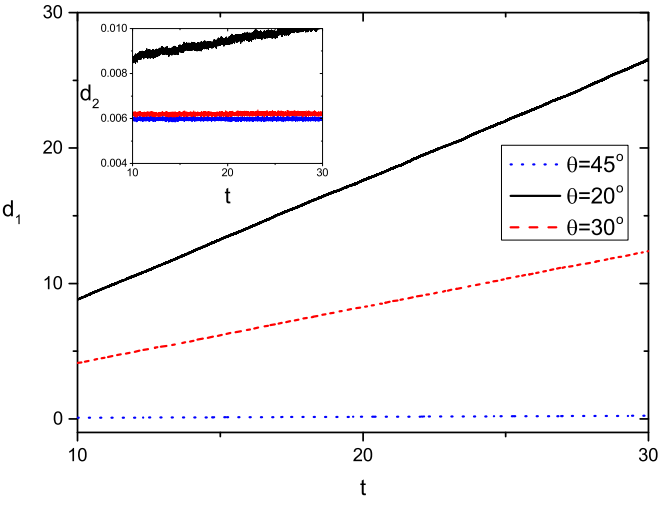

FIG. 10. (Color online) Components of mean square displacement vs time for a constant external field (Pe′ = 80). Curves from top to bottom are for $\theta = 20^\circ$, 30°, and 45°.

corresponding standard deviation, with the results shown in Table I. Since the error bars are generally smaller than the symbol size, they are not shown in the figures. For $\mathrm{Pe}' = 10$, we also use different particle numbers 50000, 100000, and 200000 to find that the trajectories hardly changes with $A/A_0 = 0.831$, 0.827, and 0.829, respectively.

The mean trajectories at $\omega = 0.1$ for $\theta = 20^\circ$ and 30° are shown in Figs. 8(a) and 8(b), respectively, in comparison with Fig. 4(a) for $\theta = 45^\circ$.

In spectral signal analysis, the trajectory is fitted by a Fourier series to give the amplitudes for different harmonics. Usually, the amplitude of the first harmonic (A_{fh}) was examined in the prior SR studies for closed systems [4–6]. We follow suit and plot the result for $\omega = 0.1$ in Fig. 9 for demonstration and comparison. Note that, when $\mathrm{Pe}' \to \infty$, the trajectory becomes a square wave with $A_{\mathrm{fh}} = 4a/\pi = 0.64$. One can see a similar trend to that in Fig. 5(a). However, when the trajectory deviates strongly from a sinusoidal wave, the amplitudes of higher harmonics may become more important. Therefore, we choose to examine $A = (C_{\max} - C_{\min})/2$ and normalize it by A_0, the value for the corresponding non-Brownian particles. In this way, one can easily judge the occurrence of an enhancement phenomenon similar to SR by checking if $A/A_0 > 1$.

For a constant external field ($\mathrm{Pe}' = 80$), we calculate d_1 and d_2, and plot them against time in Fig. 10. Apart from the result $d_1 \gg d_2$, a linear dependence on time is observed.

[1] L. Gammaitoni, P. Hanggi, P. Jung, and F. Marchesoni, Rev. Mod. Phys. **70**, 223 (1998).

[2] I. Goychuk and P. Hanggi, Phys. Rev. Lett. **91**, 070601 (2003).

[3] I. Goychuk, P. Hanggi, J. L. Vega, and S. Miret-Artes, Phys. Rev. E **71**, 061906 (2005).

[4] P. S. Burada, G. Schmid, D. Reguera, M. H. Vainstein, J. M. Rubi, and P. Hanggi, Phys. Rev. Lett. **101**, 130602 (2008).

[5] P. K. Ghosh, F. Marchesoni, S. E. Savel'ev, and F. Nori, Phys. Rev. Lett. **104**, 020601 (2010).

[6] P. K. Ghosh, R. Glavey, F. Marchesoni, S. E. Savel'ev, and F. Nori, Phys. Rev. E **84**, 011109 (2011).

[7] N. A. Kotov, Y. Liu, S. Wang, C. Cumming, M. Eghtedari, G. Vargas, M. Motamedi, J. Nichols, and J. Cortiella, Langmuir **20**, 7887 (2004).

[8] Y. Zhang, S. Wang, M. Eghtedari, M. Motamedi, and N. A. Kotov, Adv. Funct. Mater. **15**, 725 (2005).

[9] D. J. Irvine, A. Stachowiak, and S. Jain, Mater. Sci. Forum **426**, 3213 (2003).

[10] I. V. Grigoriev, Y. A. Makhnovskii, A. M. Berezhkovskii, and V. Y. Zitserman, J. Chem. Phys. **116**, 9574 (2002).

[11] A. M. Berezhkovskii, V. Y. Zitserman, and S. Y. Shvartsman, J. Chem. Phys. **118**, 7146 (2003).

[12] S. Shanbhag, J. W. Lee, and N. Kotov, Biomaterials **26**, 5581 (2005).

[13] H. Zhou, S. B. Chen, J. Peng, and C. H. Wang, J. Colloid Interface Sci. **342**, 620 (2010).

[14] K.-L. Cheng, Y.-J. Sheng, and H.-K. Tsao, J. Chem. Phys. **129**, 184901 (2008).

[15] A. M. Berezhkovskii, L. Dagdug, Y. A. Makhnovskii, and V. Yu. Zitserman, J. Chem. Phys. **132**, 221104 (2010).

[16] A. M. Berezhkovskii and L. Dagdug, J. Chem. Phys. **133**, 134102 (2010).

[17] S. B. Chen, J. Chem. Phys. **135**, 014904 (2011).

[18] S. B. Chen, J. Chem. Phys. **134**, 014902 (2011).

[19] S. B. Chen, J. Chem. Phys. **139**, 074904 (2013).

[20] H. C. Ottinger, *Stochastic Processes in Polymeric Fluids- Tools and Examples for Developing Simulation Algorithm* (Springer, Berlin, 1996).